Philosophical Magazine Letters
Publication details, including instructions for authors and subscription information:
http://www.tandfonline.com/loi/tphl20

Strength softening at shear bands in metallic glasses

Xianqi Lei [a], Yujie Wei [a], Zheng Hu [a] & Wei-Hua Wang [b]
[a] LNM, Institute of Mechanics, Chinese Academy of Sciences, Beijing, 100190, P.R. China
[b] Institute of Physics, Chinese Academy of Sciences, Beijing, 100080, P.R. China
Version of record first published: 14 Jan 2013.

To cite this article: Xianqi Lei, Yujie Wei, Zheng Hu & Wei-Hua Wang (2013): Strength softening at shear bands in metallic glasses, Philosophical Magazine Letters, 93:4, 221-230

To link to this article: http://dx.doi.org/10.1080/09500839.2012.760851

Philosophical Magazine Letters, 2013
Vol. 93, No. 4, 221–230, http://dx.doi.org/10.1080/09500839.2012.760851

Strength softening at shear bands in metallic glasses

Xianqi Lei[a], Yujie Wei[a]*, Zheng Hu[a] and Wei-Hua Wang[b]

[a]*LNM, Institute of Mechanics, Chinese Academy of Sciences, Beijing 100190, P.R. China;*
[b]*Institute of Physics, Chinese Academy of Sciences, Beijing 100080, P.R. China*

(*Received 10 October 2012; final version received 15 December 2012*)

The plasticity of metallic glasses (MGs) is mediated by localized shearing in thin bands, degrading the mechanical properties at shear bands (SBs), which can cause shear localization and poor deformability. Quantifying the strength loss at SBs in MGs is important for both further material improvement and failure prediction. By applying a combination of microscale bending with *in situ* tensile tests, we successfully determine the strength loss at SBs in two typical MGs, namely $Zr_{41}Ti_{14}Cu_{12.5}Ni_{10}Be_{22.5}$ and $(Cu_{50}Zr_{50})_{95}Al_5$, that are about 20% lower than those of their intact counterparts. We further notice, based on fractographic examinations, that stable SBs may induce only a negligible heat, but unstable SBs give rise to a high temperature increase in SBs. This observation sheds light on the controversy about whether SBs in MGs must be hot.

Keywords: metallic glasses; shear band; bending; strength softening

1. Introduction

Before materials approach their catastrophic failure point, there commonly exist some precursors. Shear localization [1], for example, is an anomaly ubiquitously observed in materials just before the applied load or deformation reaches their limits. Typical examples of such anomaly include the formation of meter-sized faults before earthquakes, micron-sized SBs in crystalline materials before rupture [1] and nanometer-wide SBs in metallic glasses (MGs) [2–5] prior to failure. In MGs, the shear localization at the initiation of plastic deformation is a key factor limiting their wider application, which otherwise can have attractive mechanical properties. On the one hand, since the plasticity of MGs at ambient conditions is mediated by SBs [6–9], it is desirable to have fine-sized SBs uniformly distributed during plastic deformation. On the other hand, in contrast to the strength of intact MGs, the strength of MGs with SBs is lower [2,3,10–15]. The degraded strength at SBs leads to progressively localized deformation, and soon results in catastrophic failure [2–5,16–18]. So far, most attention has been paid to the exploration of methods promoting the number of SBs while controlling their size in MGs during plastic deformation [19–22]. Very little is known about the properties of SBs themselves. This situation may be partly due to the difficulty of capturing the transient status change in SBs before the sample runs into final failure [16–18,23]. There is little time to probe

*Corresponding author. Email: yujie_wei@lnm.imech.ac.cn

directly the properties of SBs before their rupture. For example, to determine the temperature rise at SBs, Lewandowski and Greer [24] had to rely on an indirect but effective strategy of coating the surface of MGs with a layer of material of low melting temperature. The temperature rise at SBs was then deduced from the melted zones of the coating material in the post-mortem samples. Zhang et al. [25] also applied this fusible coating method to a wide range of MGs. We note that there exists a good understanding of strength softening at SBs in MGs [2,3,10–15, 26,27]. Indentation tests also confirm that the hardness in the vicinity of SBs is lower than that in the intact region [14–15]. However, existing indentation experiments have been conducted with typical indenter size on the order of several microns, which is nearly three orders of magnitude larger than the width of a shear band in metallic glasses (around 10 nm in thickness [2,3]). Hardness measurements by indentation cannot represent the intrinsic strength in a single shear band. A direct method to measure the shear strength in a SB is unfortunately not available. Here, we utilize a combination of micro-scale bending with *in situ* tensile tests, and successfully determine the strength at SBs in MGs. Bending is first employed to MG plates to produce stable SBs; we then perform tensile tests on the samples with pre-existing SBs to abstract the strength at SBs.

2. Methods and results

The bending of thin plates is particularly useful and widely used for studies of SBs since the propagation of SBs ceases as they approach the neutral plane, and early catastrophic failure is avoided, permitting substantial deformability when the samples are sufficiently thin [28–33]. Here by utilizing the SBs formed after bending but before the rupture of the material, we continue to perform *in situ* tensile tests with the bent samples, and then derive the strength loss at SBs in MGs after obtaining the strength of samples with pre-existing SBs. Two types of typical MGs, the commercially available $Zr_{41}Ti_{14}Cu_{12.5}Ni_{10}Be_{22.5}$ (Vitreloy 1) and $(Cu_{50}Zr_{50})_{95}Al_5$, have been tested in the present work. Figure 1 shows the dimensions of the samples. To ensure good curvature control in the bending region, we designed a bending rig shown in Figure 1b. The bent samples are then mounted to an *in situ* micro-tensile testing system shown in Figure 1c. To eliminate possible bending effects while applying tension, we use pins to hold the two ends of the samples, and allow them to rotate freely in both the *y*- and *z*-axes. Owing to irreversible plastic strain accommodated by the SBs, the samples after bending are usually curved, and there are many conjugated SBs at both the top and the bottom sides of the sample, as seen in Figure 1d.

In Figure 2a, we show a typical tensile stress vs. displacement curve for a bent sample of Vitreloy 1. A pre-bending ratio of $H/R = 0.1$ was applied to the sample before tension, where H is the plate thickness (see Figure 1a) and R is the radius of the indenter of the bending rig (Figure 1b). The initial slow increase in stress arises from the straightening of the curved sample, as seen in Figure 2b. When the tensile stress reaches 267 MPa (point '*b*' keyed in the stress-displacement curve in Figure 2a), the sample is completely straight. At this stress level, there is nearly no extension for those pre-existing SBs, as seen in the deformation pattern shown in Figure 2c. After point '*b*' in Figure 2a, a steep slope in the stress-displacement curve emerges. By comparing the deformation patterns in Figure 2c and 2d, we see clearly the growth of SBs as the

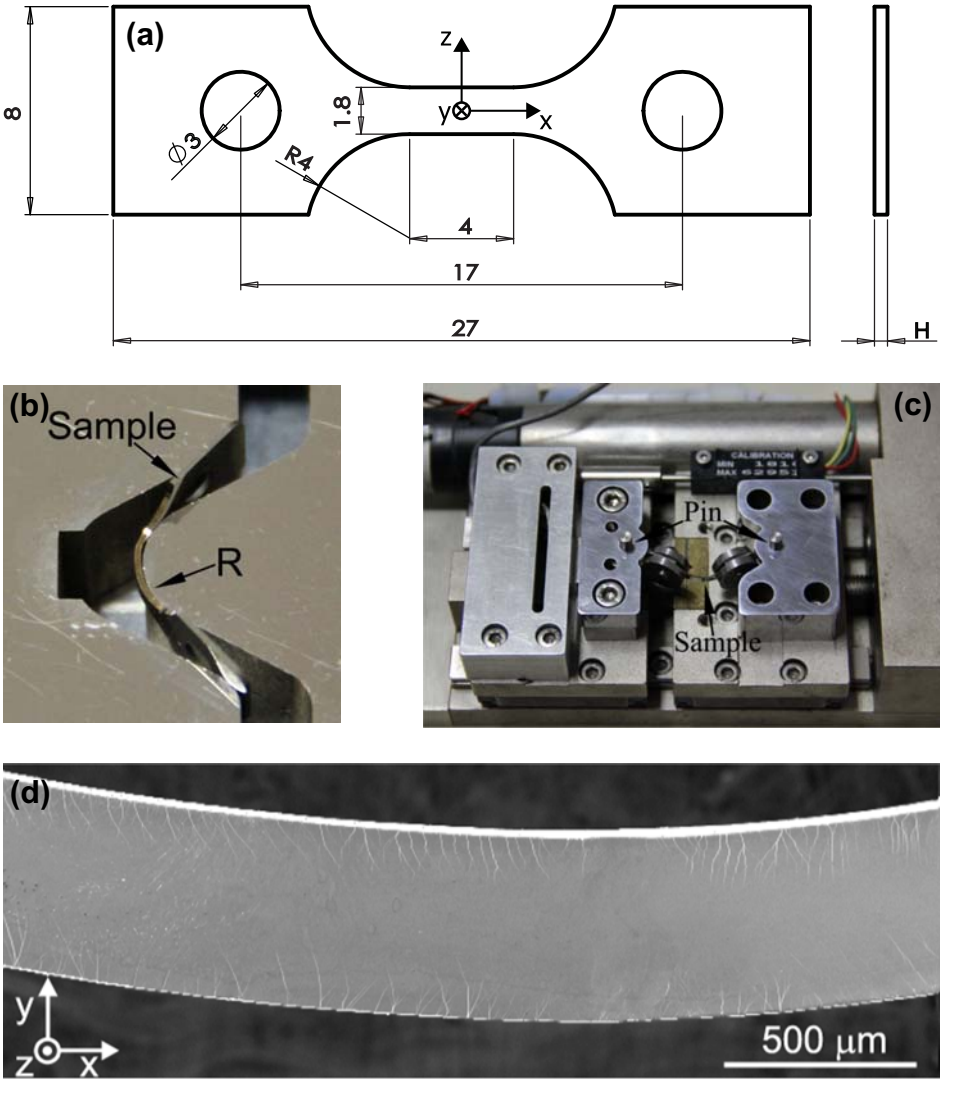

Figure 1. (colour online) The experimental set-up for the microscale bending and tensile tests. (a) sample dimensions. The thickness H of the samples varies slightly around 0.4 mm. (b) close-up view of the indenter for bending experiments. (c) set-up for the tensile tests. (d) whole view for a typical sample after bending, where SBs were seen.

tensile stress approaches the maximum strength (1652 MPa) of the sample. Coalescence of growing SBs from the top and the bottom leads to the final failure, as shown in Figure 2e. Such scenarios observed in Vitreloy 1 are also seen in our experiments for a bent sample of $(Cu_{50}Zr_{50})_{95}Al_5$, as detailed in Figure 3. Figure 3a gives the stress-displacement curve in the $(CuZr)_{95}Al_5$ sample with a pre-bending ratio of $H/R = 0.1$. The respective deformation patterns at the stress levels marked in Figure 3a are shown in Figure 3b–d, where the growth and coalescence of SBs are also clearly observed. The

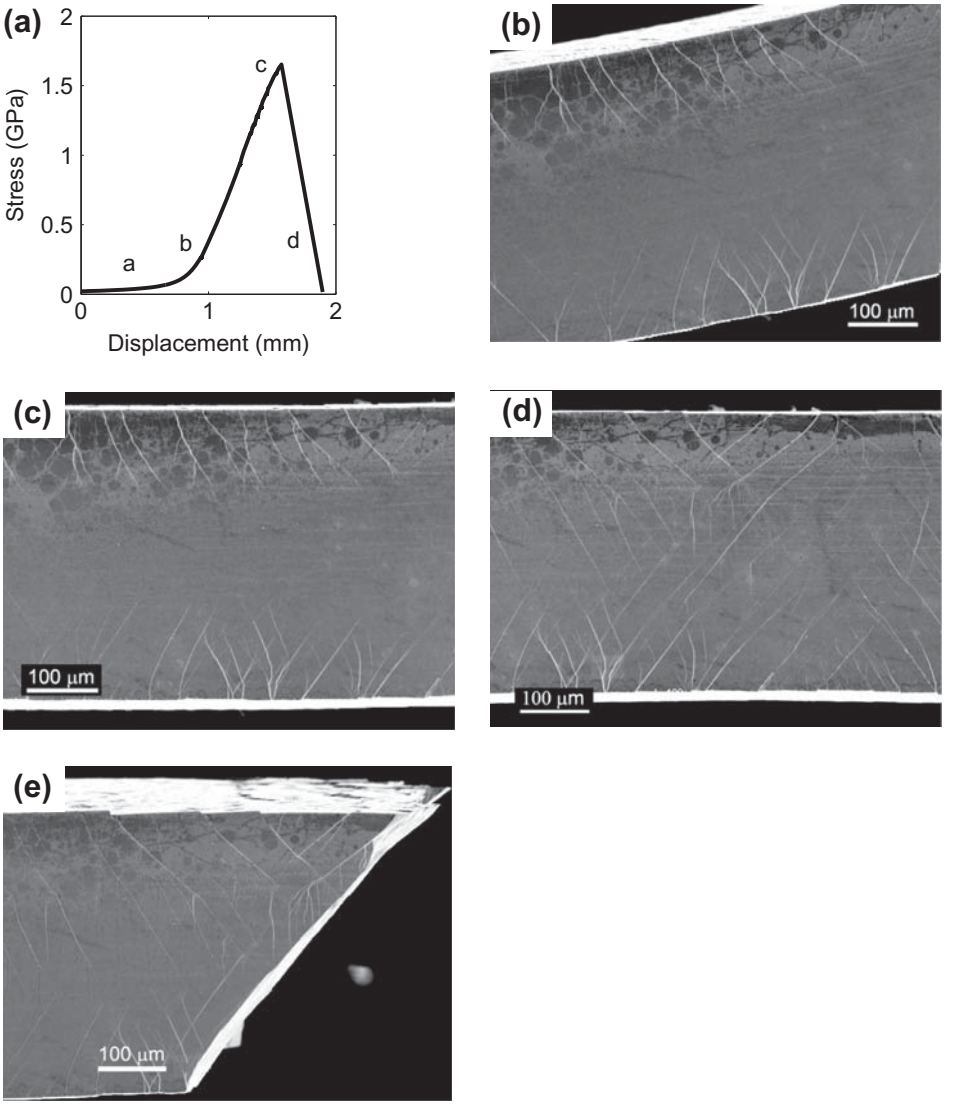

Figure 2. *In situ* tensile tests and scanning electron microscopy of shear bands in pre-bent Vitreloy 1. (a) stress-displacement curve of the pre-bent plates with bending ratio $H/R = 0.1$. (b)–(e), Side view showing the evolution of SBs at different stress levels. (b) Initial SB structures (point '*a*' in (a)). (c) Straightened sample at the applied stress of 267 MPa ('b' in (a)). (d) The growth of SBs as tensile stress reaches the maximum strength of 1652 MPa ('c' in (a)). Coalescence of SBs from the top and bottom sides is observed. (e) Final failure pattern ('d' in (a)).

final failure pattern in Figure 3d also suggests that the fracture surface is guided by the original SBs left by pre-bending.

Given that by pre-bending, SBs do not transverse the sample, the measured strength σ_m for bent samples is controlled by both the strength in the intact region (σ_c) and that at the SBs (σ_{sb}). In order to obtain the strength σ_{sb} in SBs, we need to determine the

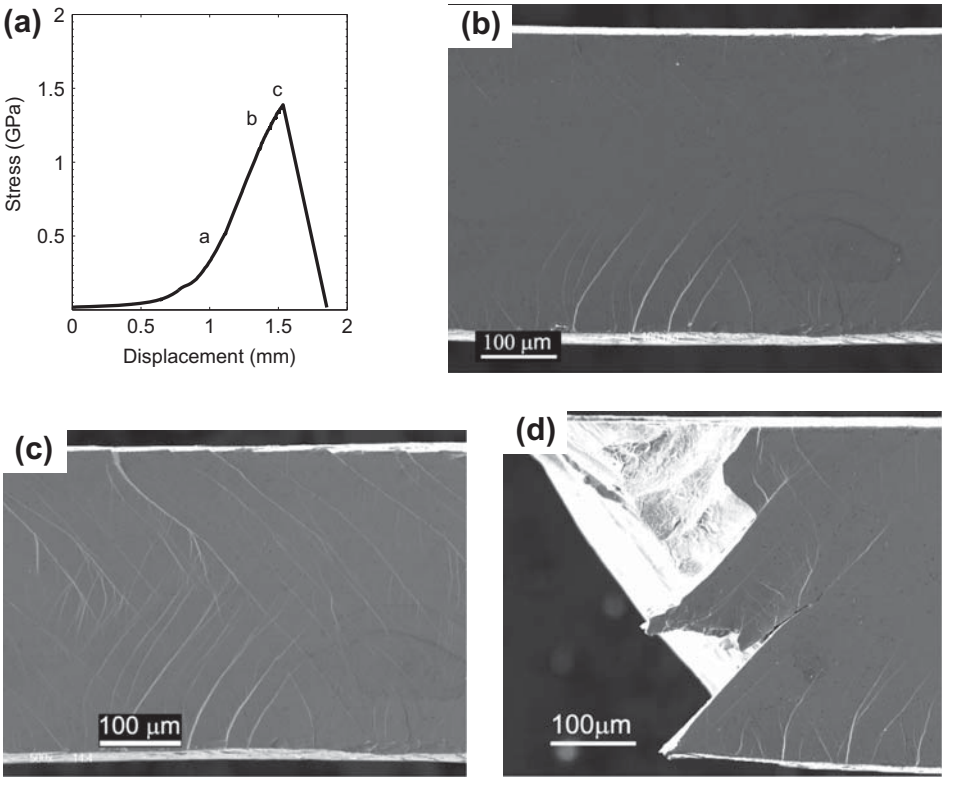

Figure 3. *In situ* microscale tensile tests and scanning electron microscopy of shear bands in pre-bent $(CuZr)_{95}Al_5$. (a) stress-displacement curve of the plate with bending ratio $H/R = 0.1$. (b) straightened sample, corresponding to point '*a*' in (a). (c) SB pattern as the tensile stress reaches nearly the maximum strength of 1389 MPa ('*b*' in (a)). Coalescence of growing SBs from the top and the bottom is also observed. (d) The final failure pattern ('*c*' in (a)).

SB length at a given bending ratio. With the approximation of plane strain bending (which is the case here since the sample width is at least four times larger than the thickness H, as seen in Figure 1a, the characteristic length of a SB (projected length along the plate thickness) is obtained by calculating the distance from the neutral plane at which the stress reaches the critical value σ_c for SB initiation [28–30,33], which is given as

$$\frac{a}{R} = \frac{H}{2R} - (1 - \nu)\frac{\sigma_c}{2\mu}, \tag{1}$$

where μ is the shear modulus and ν is the Poisson's ratio of the MG. We apply the mixing law to write σ_m as $\sigma_m = \xi\sigma_{sb} + (1 - \xi)\sigma_c$, where $\xi = 2a/H$. For the special case of $\xi = 0$, i.e. no SBs exist, we have $\sigma_m = \sigma_c$; as $\xi \to 1$, $\sigma_m \approx \sigma_{sb}$. The mixing law assumes that when the final fracture surface yields, both the portion with pre-existing SBs and the intact part reach their respective strengths. This assumption smears out any possible stress concentration at the tip of SBs. Unlike crystalline materials, where the

Table 1. The mechanical properties of $Zr_{41}Ti_{14}Cu_{12.5}Ni_{10}Be_{22}$ and $(Cu_{50}Zr_{50})_{95}Al_5$. Their strengths σ_{sb} at shear bands are also given, which are about 20% lower than the strengths of their respective intact counterparts.

Material	G (GPa)	ν	σ_c (GPa)	σ_{sb} (GPa)	Strength loss
$Zr_{41}Ti_{14}Cu_{12.5}Ni_{10}Be_{22.5}$	36.2[21,28]	0.341[21,28]	1.86	1.42	23%
$(Cu_{50}Zr_{50})_{95}Al_5$	32.3[33]	0.372[33]	1.78	1.35	24%

strengths of perfect regions and defective parts can differ by several orders of magnitude, the structures in MGs are rather uniform except at the sub-nanometre length scale [34], and there is no significant strength difference between the sheared region and the intact part. Therefore, in contrast to the crystalline counterpart, there is no mechanism to support high-level stress concentration at the tip of a SB in MGs. With Equation (1), we then write the measured strength as,

$$\sigma_m = \sigma_{sb} + (\sigma_c - \sigma_{sb})(1-\nu)\frac{\sigma_c}{\mu}\frac{R}{H}. \quad (2)$$

With Equation (2) and material parameters given in Table 1, we show in Figure 4a the measured strength σ_m for pre-bent Vitreloy 1 samples at different bending ratios. The trend can be well characterized by Equation (2). The solid line is the least-squares fitting results to the experimental data with $\sigma_{sb} = 1.42$ GPa. This value is about 23% lower than σ_c – the tensile strength of the intact Vitreloy 1 samples from our measurement. Corresponding results for $(Cu_{50}Zr_{50})_{95}Al_5$ are shown in Figure 4b. Now, the solid line is obtained with $\sigma_{sb} = 1.35$ GPa, and the strength softening at SBs is about 24%.

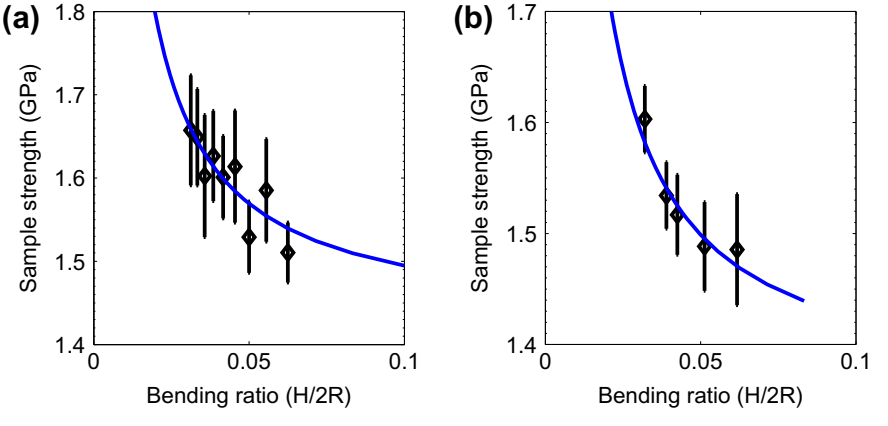

Figure 4. (colour online) Measured strength for pre-bent samples at different bending ratio vs. the theoretical fitting by using Equation (2). Note that $H/2R$ in the x-axis corresponds to the maximum strain in the sample subjected to bending. (a) Results for Vitreloy 1 (symbols are from experiments and the solid line comes from theoretical fitting). (b) Results for $(Cu_{50}Zr_{50})_{95}Al_5$. The average of five independent measurements at each bending ratio is used in the plot. The error bars represent the standard deviation of the five measurements.

Given that all experiments are performed at room temperature, the strength loss in SBs observed here is a result of the structure change in SBs, either by shear-induced dilatation [10–15,26] or nano-sized damage in SBs [2,3], but not by thermal softening since there is sufficiently long time for thermal diffusion after bending but before tension.

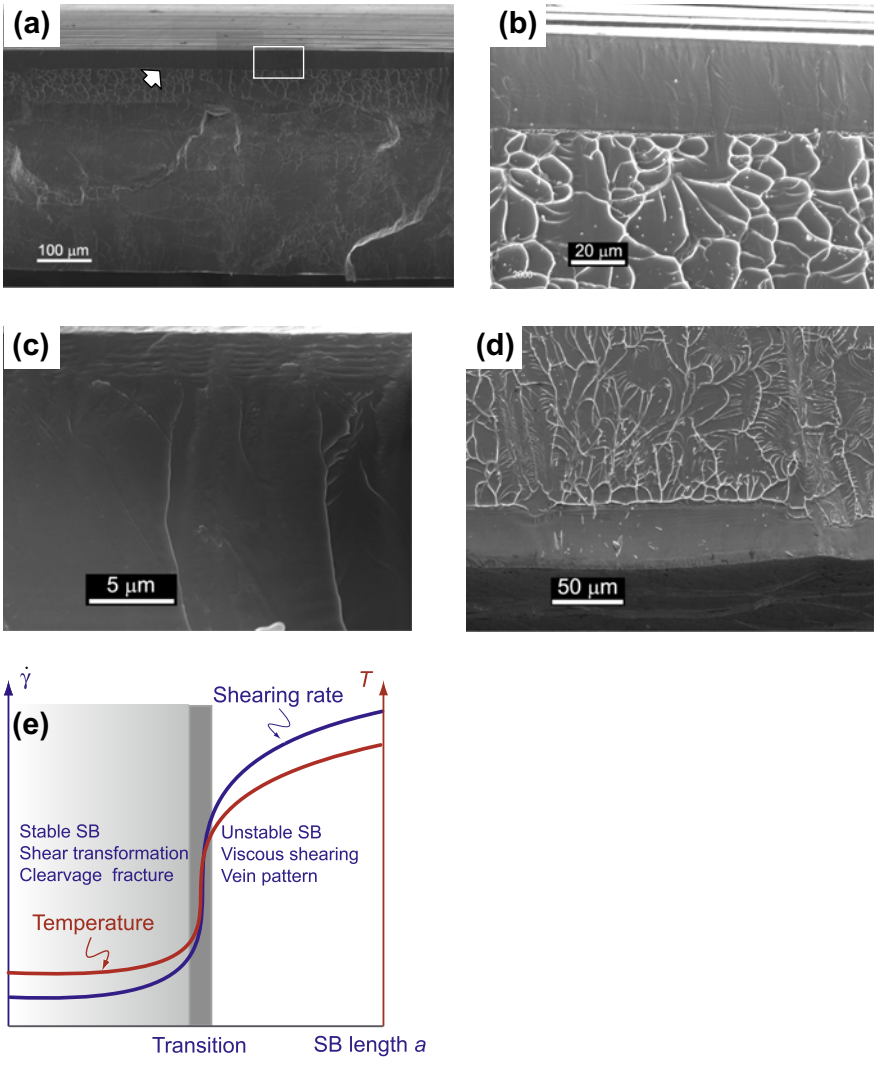

Figure 5. (colour online) Scanning electron microscopy of fracture surfaces. (a) The whole view of fracture surface of a Vitreloy 1 sample with pre-bending $H/R = 0.1$. At the top (guided by the white arrow), we see a flat region with height about 50 μm. (b) Close-up of the boxed region in (a) showing the clear discrepancy in fracture surfaces: a transition of the flat region at the top to vein structures below. (c) Further amplification of the top region in (b) showing striation in fracture surfaces. Fracture surface of $(Cu_{50}Zr_{50})_{95}Al_5$ in (d) also shows the contrast of flat region vs. vein patterns, which is similar to what we see for Vitreloy 1 in (b). (e) Illustration to the stable to unstable transition during SB propagation, and corresponding changes in shearing rate in SBs, temperature rise in SBs, deformation mechanism and patterns in fracture surfaces.

By checking closely the failure patterns in those pre-bent samples (see Figure 5a for a whole view of the fracture surface of Vitreloy 1), we find that the surfaces exhibit three featured regions. In contrast to the vein structures, we normally observed in the fracture surfaces of MGs, the top part here (see Figure 5b) is very flat, as also shown in the close-up view in Figure 5c. Shear offset is around tens of microns in samples with a thickness about 0.4 mm. In the flat region, it is further noted that there are striations in the top-most part (Figure 5c). This type of striation has been observed in fatigue tests [35–37] for MGs and in bent MG wires [38–39]. The characteristics of such fracture surfaces are robustly seen in most samples we tested. In Figure 5d, we also show similar features seen in the fracture surfaces of $(Cu_{50}Zr_{50})_{95}$ samples.

3. Discussion and conclusions

The patterns of fracture surfaces in pre-bent samples seen in Figure 5 are intriguing. Typical vein patterns seen in fracture surfaces of MGs are believed to be a resultant from shear-induced viscous flow in thin bands. Quick heat generation by localized plastic dissipation and the delayed heat diffusion in those bands are regarded as the origins of vein formation. In such scenarios, inside the narrow SBs, there is a stationary balance of heat diffusion and heat source, resulting from plastic work in the band as [1]

$$\kappa\frac{\partial^2 T}{\partial x^2}+\frac{\beta\tau\dot{\gamma}}{\rho C}=\frac{\partial T}{\partial t}\approx 0, \tag{3}$$

where T is the temperature, τ is the shear stress, $\dot{\gamma}$ is the shear strain rate in the band, ρ is density, C is the specific heat, κ is the thermal diffusion, β is the converting coefficient and is slightly smaller than unit, and x and t are respectively the coordinate varying along band thickness and time. Then, the band width should be $\delta_{asb}\approx\sqrt{\rho C\kappa T/\beta\tau\dot{\gamma}}$ [1,40], and the temperature rise in SBs can be derived as $T=\beta\delta_{asb}^2\tau\dot{\gamma}/\rho C\kappa$. Along this line, the estimated temperature rise at SBs in MGs is only several K, differing by several orders of magnitude from those by experimental measurements [23,26,37,41–45]. This striking difference could stem from the inaccurate estimate for $\dot{\gamma}$ in the band and the apparent discrepancy for plastic deformation mechanisms between MGs and their crystalline counterparts. Based on the experimental observation given in Figure 5, we suspect that during quasi static SB propagation and before rupture of the sample, short-range shear transformation [46,47] may be the dominant mechanism for plastic deformation. Relatively low shearing rate at this stage gives rise to a small temperature rise at SBs, and the strength softening at SBs in MGs observed here is attributed to shear-induced dilatation or nano-sized damage in thin bands. In the absence of excessive heating, the fracture surface formed under this condition is rather smooth, and resembles that from cleavage fracture. In contrast, the heat generation during rupture in SBs, arising from the coalescence of shear transformation zones and the acceleration of shearing rate, is enormous and can induce a substantial drop in viscosity by thermal softening. It hence causes the formation of broadly observed vein structures. A detailed illustration for such changes is given in Figure 5e. Our experimental observations given in Figure 5, combined with the above hypothesis, pave the way to reconcile the remaining controversy about whether SBs must be hot [23,26,37,41–44,48].

Acknowledgements

The authors acknowledge support from the Chinese Academy of Sciences (Hundred Talent Programme), NSFC (11021262) and MOST 973 of China (No. 2012CB937500) for YW, from MOST 973 of China (No. 2010CB731603) and NSFC (50921091) for WHW. The authors are grateful to Professor Yilong Bai for fruitful discussion, to Dr Jijia Xie, Dr Guihua Duan and Dr Duanyi Li for their assistance with *in situ* experiments. The authors are also grateful to Professor E. A. Davis for proofreading this paper.

References

[1] Y. Bai and B. Dodd, *Adiabatic Shear Localization: Occurrence, Theories, and Applications*, Pergamon Press, Oxford, 1992.
[2] E. Pekarskaya, C.P. Kim and W.L. Johnson, J. Mater. Res. 16 (2001) p.2513.
[3] J. Li, F. Spaepen and T.C. Hufnagel, Phil. Mag. A 82 (2002) p.2623.
[4] Y. Zhang and A.L. Greer, Appl. Phys. Lett. 89 (2006) p.071907.
[5] W.H. Jiang and M. Atzmon, Scripta Mater. 54 (2006) p.333.
[6] A.L. Greer, Science 267 (1995) p.1947.
[7] W.L. Johnson, MRS Bull. 24 (1999) p.42.
[8] A. Inoue, Acta Mater. 48 (2000) p.279.
[9] C.A. Schuh, T.C. Hufnagel and U. Ramamurty, Acta Mater. 55 (2007) p.4067.
[10] L. Anand and C. Su, J. Mech. Phys. Solids 53 (2005) p.1362.
[11] D. Klaumunzer, A. Lazarev, R. Maass, F.H.D. Torre, A. Vinogradov and J.F. Loeffler, Phys. Rev. Lett. 107 (2011) p.185502.
[12] M.Q. Jiang and L.H. Dai, Acta Mater. 59 (2011) p.4525.
[13] Q.P. Chao, J.W. Liu, K.J. Yang, F. Xu, Z.Q. Yao, A. Minkow, H.J. Fecht, J. Ivanisenko, L. Y. Chen, X.D. Wang, S.X. Qu and J.Z. Jiang, Acta Mater. 58 (2010) p.1276.
[14] H. Bei, S. Xie and E.P. George, Phys. Rev. Lett. 96 (2006) p.105503.
[15] J. Pan, Q. Chen, L. Liu and Y. Li, Acta Mater. 59 (2011) p.5146.
[16] S.X. Song and T.G. Nieh, Intermetallics 19 (2011) p.1968.
[17] S.X. Song, X.-L. Wang and T.G. Nieh, Scripta Mater. 62 (2010) p.847.
[18] B. Yang, M.L. Morrison, P.K. Liaw, R.A. Buchanan and G.Y. Wang, Appl. Phys. Lett. 86 (2005) p.141904.
[19] G. He, J. Eckert, W. Löser and L. Schultz, Nature Mater. 2 (2003) p.33.
[20] J. Schroers and W.L. Johnson, Phys. Rev. Lett. 93 (2004) p.255506.
[21] J.J. Lewandowski, W.H. Wang and A.L. Greer, Phil. Mag. Lett. 85 (2005) p.77.
[22] M.D. Demetriou, M.E. Launey, G. Garrett, J.P. Schramm, D.C Hofmann, W.L. Johnson and R.O. Ritchie, Nature Mater. 10 (2011) p.123.
[23] Y.Q. Cheng, Z. Han, Y. Li and E. Ma, Phys. Rev. B 80 (2009) p.134115.
[24] J.J. Lewandowski and A.L. Greer, Nature Mater. 5 (2006) p.15.
[25] Y. Zhang, N.A. Stelmashenko, Z.H. Barber, W.H. Wang, J.J. Lewandowski and A.L. Greer, J. Mater. Res. 22 (2007) p.419.
[26] M. Zhao and M. Li, Scripta Mater. 65 (2011) p.493.
[27] C.-K. Huang and J.J. Lewandowski, Metal. Mater. Trans. A 43A (2008) p.2687.
[28] R.D. Conner, W.L. Johnson, N.E. Paton and W.D. Nix, J. Appl. Phys. 94 (2003) p.904.
[29] R.D. Conner, Y. Li, W.D. Nix and W.L. Johnson, Acta Mater. 52 (2004) p.2429.
[30] G. Ravichandran and A. Molinari, Acta Mater. 53 (2005) p.4087.
[31] A.H. Brothers and D.C. Dunand, Adv. Mater. 17 (2005) p.484.
[32] G. Kumar, A. Desai and J. Schroers, Adv. Mater. 23 (2011) p.461.
[33] Y. Wei, X. Lei, L.S. Huo, W.H. Wang and A.L. Greer, Mater. Sci. Eng. A 560 (2013) p.510.

[34] H.W. Sheng, H.Z. Liu, Y.Q. Cheng, J. Wen, P.L. Lee, W.K. Luo, S.D. Shastri and E. Ma, Nature Mater. 6 (2007) p.192.
[35] P.A. Hess, B.C. Menzel and R.H. Dauskardt, Script. Mater. 54 (2006) p.355.
[36] G.Y. Wang, P.K. Liaw, Y. Yokoyama, A. Inoue and C.T. Liu, Metal. Sci. A 494 (2008) p.314.
[37] H. Zheng and Y. Li, J. Mater. Res. 24 (2009) p.3620.
[38] X.K. Xi, D.Q. Zhao, M.X. Pan, W.H. Wang, Y. Wu and J.J. Lewandowski, Phys. Rev. Lett. 94 (2005) p.125510.
[39] G. Wang, D.Q. Zhao, H.Y. Bai, M.X. Pan, A.L. Xia, B.S. Han, X.K. Xi, Y. Wu and W.H. Wang, Phys. Rev. Lett. 98 (2007) p.235501.
[40] Y.L. Bai, J. Mech. Phys. Solids 30 (1982) p.195.
[41] H.A. Bruck, A.J. Rosakis and W.L. Johnson, J. Mat. Res. 11 (1996) p.503.
[42] C.T. Liu, L. Heatherly, D.S. Easton, C.A. Carmichael, J.H. Schneibel, C.H. Chen, J.L. Wright, M.H. Yoo, J.A. Horton and A. Inoue, Metall. & Mater. Trans. A 29a (1998) p.1811.
[43] K.M. Flores and R.H. Dauskardt, J. Mater. Res. 14 (1999) p.638.
[44] W.J. Wright, R.B. Schwarz and W.D. Nix, Mater. Sci. Eng. A 319 (2001) p.229.
[45] G.Y. Wang, Q.M. Feng, B. Yang, W.H. Jiang, P.K. Liaw and C.T Liu, Intermetallics 30 (2012) p.1.
[46] F. Spaepen, Acta Metall. 25 (1977) p.407.
[47] A.S. Argon, Acta Metall. 27 (1979) p.47.
[48] F. Spaepen, Nature Mater. 5 (2006) p.7.